NEDE–24520
Class I
March 1978

RIGID AND FLEXIBLE VENT HEADER TESTING IN THE QUARTER SCALE TEST FACILITY

MARK I CONTAINMENT PROGRAM, TASK 5.3.3

W. Kennedy
D. McGovern
R. Maraschin
K. Wolfe

Approved: Ray Lundberg

R. E. Lundberg
Manager, Nuclear Engineering
Alternate Energy Division
Acurex Corporation

Approved: Howard L Morse

H. L. Morse
General Manager
Alternate Energy Division
Acurex Corporation

Prepared for
General Electric Company
Nuclear Energy Engineering Division
175 Curtner Avenue
San Jose, California 95125

Acurex Corporation
Alternate Energy Division

DISCLAIMER OF RESPONSIBILITY

This document was prepared by or for the General Electric Company. Neither the General Electric Company nor any of the contributors to this document:

A. Makes any warranty or representation, express or implied, with respect to the accuracy, completeness, or usefulness of the information contained in this document, or that the use of any information disclosed in this document may not infringe privately owned rights; or

B. Assumes any responsibility for liability or damage of any kind which may result from the use of any information disclosed in this document.

TABLE OF CONTENTS

LIST OF TABLES

LIST OF ILLUSTRATIONS

ABSTRACT

Sixteen tests were conducted in the G.E. Quarter-scale Test Facility to study the effects of vent header flexibility on Mark I vent header impact loads caused by pool swell from a postulated loss of coolant accident. The first eight tests were conducted with a rigid vent header model; the remaining tests used a flexible model with ovalling stiffness approximately scaled for the Quarter-scale Facility. Both high- and low-impact conditions were studied. These conditions were produced by varying the drywell pressurization rate and the initial drywell-to-torus pressure difference (which controls the initial water level in the downcomers).

Vent header loads were measured by a load cell and by eight flush-mounted pressure transducers distributed around the impact zone. The output from the pressure transducers provided details of the transient impact pressure distribution on the bottom quadrant of the vent header. Compared to the rigid vent header, the flexible vent header reduced the magnitude of the peak impact load and shifted the peak later in time. Local pressures generally were lower for the flexible cylinder.

1. INTRODUCTION

Mark I vent header impact loads due to pool swell from a postulated loss of coolant accident (LOCA) developed in earlier programs were based on water impact to a rigid cylinder. Because the vent header is relatively flexible, some load reduction would be expected to occur as the vent header wall moves away from the impact. This program was conducted to assess the influence of vent header flexibility on impact loads.

Objectives of the program were: a) to determine the magnitude of reduction of vent header impact load due to flexibility by comparing the impact loads measured with a rigid and scaled flexible quarter-scale vent header, and b) to measure the transient pressure profile on the quarter-scale vent header.

The vent loads from the rising suppression pool are impact loads caused by momentum exchange between the water and the vent cylinder. When a body accelerates in a fluid or vice versa, the body and the fluid exchange momentum, establishing the steady-state flowfield. If the cylinder is completely immersed, for example, classical hydrodynamics predicts the impulse, I, required to accelerate a cylinder of diameter D and length L from 0 to V to be:

$$I = V(\pi/4\ D^2 L \rho_{fluid}) \qquad (1\text{-}1)$$

The term $(\pi/4\ D^2 L \rho_{fluid})$ is called the hydrodynamic mass and, for the cylinder, is equal to the displaced water mass. However, when a cylinder impacts a water surface, the problem is more complicated. Von Karman (Reference 1) evaluated seaplane float impacts during landing and arrived at a theoretical impulse value equal to half that given by equation 1 for cylinders impacting a flat water surface.

Experimental work on cylinders impacting a water surface was performed by NASA (Reference 2), the U.S. Navy (Reference 3), and GE (Reference 4). These experiments show impact impulses of 20 to 25% of fully submerged values. The vent header impact evaluation differs from that referenced above due to the curved surface of the pool and the presence of the two submerged bubbles.

Testing has been conducted to simulate the fluid dynamic events of pool swell due to a postulated loss of coolant accident. These tests have measured the vent header impact loads in Twelfth and Quarter Scale using essentially rigid members to simulate the vent header structure (References 5 and 6). Figure 1-1, taken from a typical Quarter-scale test, shows the shape of the pool and bubbles at impact. The pool surface is crowned in the direction normal to the plane of Figure 1-1.

Quarter-scale and Twelfth-scale vent header impulse values generally agree with the results of References 2, 3 and 4 (impulse values of 20% of fully submerged value) but cannot be correlated by pool swell velocity alone, indicating the influence of pool and bubble geometry.

GE Company Proprietary

Figure 1-1
Quarter-scale Pool Surface As a Function of Time (Large Orifice, 0 ΔP)
(GE Company Proprietary)

In actual containment configurations, the vent header assembly is a thin shell structure (D/t ratio of 113 to 232). This structure permits transient deformations which modify the load and the forces transmitted through the system supports. The flexibility allows the impacted surface to "run away" from the impact, and thus modify it.

To measure the influence of this deformation on the loads, the rigid and flexible vent header testing was undertaken. Impact loads were measured for a rigid and flexible model of the vent header using the Quarter-scale Test Facility. The flexible model has approximately the same ovalling deformation history as a model rigidly supported at each end, with proper scaled length between supports. A vent header support system was designed to react the vertical component of the impact, but allow free ovalling expansion of the header. Rigid loads were obtained from a rigid vent header which fit the same support system used for the flexible cylinder. The program also provided a detailed map of the transient pressure pulse on the vent header. Because the Quarter-scale Test Facility properly scales the prototype hydrodynamics, the loads and pressure map account for the influence of 1) three-dimensional pool surface (crowning), 2) presence of the downcomer air bubbles, and 3) vent header flexibility.

Eight high-frequency, flush-mounted pressure transducers were distributed over a lower quadrant of both the rigid and flexible model to map the impact distribution. Reaction loads were measured by a load cell. The test matrix covered one value of D/t and two values of water impact speed (obtained by varying both drywell pressurization rate and the initial drywell-to-torus pressure difference, ΔP).

2. SUMMARY OF RESULTS

The general effect of flexibility is to

1) Modify the shape of the loading history obtained by pressure integration to a lower magnitude and longer duration (Figure 2-1)

2) Reduce the peak values of impact pressure at a given location.

These tests were run with the vent loss coefficient (fl/D) split between the vent and downcomer. No change in torus download was observed compared to earlier QSTF results where all the fL/D was in the downcomers.

GE Company Proprietary

Figure 2-1
Impact Pressure Load Obtained from Pressure Integration
(GE Company Proprietary)

3. TEST DESCRIPTION

The Rigid and Flexible Vent Header tests were conducted in the Quarter-scale Pool Swell Test Facility located in the Acurex Nuclear Safety Laboratory. A brief description of the Quarter-scale Test Facility and a detailed discussion of the design and instrumentation of the rigid and flexible vent headers are given below.

3.1 QUARTER-SCALE TEST FACILITY

The configuration of the Quarter-scale Test Facility, shown in Figure 3-1, is based on a Mark I BWR containment. The dimensions, however, are scaled from the G.E. twelfth-scale facility rather than a particular plant. The facility models a two-dimensional segment of the torus, containing one pair of downcomers. Drywell pressurization is modeled by partially discharging a large compressed air reservoir into a simulated drywell. A fast-acting valve and a restricting orifice are used to achieve the proper scaled drywell pressurization rate.

Transparent end and side ports allow high-speed (500 frames per second) photographs to be taken of each test. From the photographic data the pool surface velocities, exact time of vent header impact, and details of the vent clearing phenomenon can be determined.

For these tests the facility's basic instrumentation consisted of the following (see Figure 3-2):

- Drywell charging orifice upstream pressure (P14)
- Drywell pressure (P11)
- Torus pressure (several locations)
- Torus load cell and accelerometer (to measure vertical torus force)
- Vent header load cell and accelerometer

During a test, data are obtained from this instrumentation at a combined rate of 20 kHz with an analog-to-digital converter. Data are printed, plotted (usually within a few hours of a test), and recorded on a floppy disc and magnetic tape.

In addition to the instrumentation listed above, the vent headers were equipped with pressure transducers and strain gauges as described in Section 3.4. Data from these sensors were recorded on FM tape and digitized after the test.

3.2 fL/D

GE Company Proprietary

A split-orifice system was designed with a single orifice plate at the entrance from the drywell to the vent and an orifice in each downcomer in the same location as in previous testing. The size of these losses was experimentally adjusted to yield the above values.

3.3 VENT HEADER AND SUPPORT DESIGN

The principal design basis for the header model is that under dynamic pool swell loading the displacement and deformed shape of the model be representative of scaled prototype behavior. Exact scaling cannot be achieved since the prototype vent header is a relatively long cylinder supported at each end and the Quarter Scale Facility is a two-dimensional model representing approximately 1/3 of the unsupported vent header length.

It was assumed that the prototype vent header responded to pool swell impact loads as a long cylinder in bending. For long cylinders in bending

at distances away from end affects the shear flow around the circumference of the cylinder at any cross section is VQ/I where V is total lateral shear, Q is the area moment, $A\bar{y}$, above the beam section under consideration and I is the cross sectional moment of inertia. Hence a two-dimensional model support system was sought which would create a circumferential bending moment distribution closely approximating that created by VQ/I shear flow.

The selected system is shown in Figure 3-3. The thin walled model cylinder is locally stiffened by longitudinal side plates which extend 10° above and below the horizontal centerline. Vertical impact loads to the cylinder are reacted at 4 points on the side plates by 4 swing arms which are stiff vertically but are pivoted to allow free ovalling expansion.

A static, finite element analysis of the model with side plates was performed assuming the pressure loading, $P = P_{max} \cos 2\phi$ for $-45° < \phi < 45°$ ($\phi = 0$ is bottom dead center). The chosen 80° to 100° side plate configuration results in a maximum bending moment within 1% of the VQ/I shear flow case at bottom dead center, 0°. At 75°, the 80° - 100° configuration bending moment is 26% higher than the VQ/I case.

A three-dimensional dynamic finite element analysis of the vent header without downcomers was performed to predict the ovalling response near center-span of the vent header. Using a two-dimensional dynamic analysis of the model vent header with the side plates, material type and thickness were altered until the maximum deflection and time of maximum deflection at bottom dead center agreed with the results of the three-dimensional analysis.

Figures 3-4 and 3-5 show the results of this analysis for various thicknesses of aluminum and tin. Values of time and displacement are for prototype scale. Based on these analyses, a model vent header using .090 in aluminum was constructed and a backup model of .093 tin was also constructed. The aluminum model was used for the testing.

The first ovalling frequency of the flexible vent header model was estimated to be 50-60 Hz and it was important to keep the support system natural frequency as high as possible to reduce the dynamic amplification from the support system. The existing quarter-scale load cell and support system was estimated to have a natural frequency of approximately 110 Hz with the new and lighter vent header models. A 200-Hz or greater natural frequency requirement was applied to any new series support element, such as the swing arms, so that the combined support system natural frequency would not be significantly lowered from its estimated value of 110 Hz.

The swing-arm support system was coupled to the flexible header side plates with a spherical ball joint and joined to the load cell support with needle bearings. The swing arms are curved to keep the transmitted load and the reaction force vertically in line with one another. The upper ends of the arms (pivot end) were attached to the main cylindrical column carrying the load cell, through four stiff cantelever beams made of square structural tube with external stiffening. The main cylindrical column was restrained vertically by the load cell. The column was restrained laterally by three sets of camfollower bearings located 120° apart along the column length.

The ends of the header were sealed by flexible caps of 1/16 inch thick neoprene rubber bonded in place, allowing the header to deform without significant end effects. The pressure load on the end caps was taken up by the windows of the torus section, which were located about 1/4 inch from the end caps.

Since the deformed shape required the top of the ring header model to move, a sliding, "O"-ring-sealed connection between the model and the vertical load tube was made.

For the aluminum flexible model, the downcomer wall thickness for the 45° sections and vertical sections up to the orifice plate was .083 aluminum. The orifice plate holder and lower region of the downcomer were adjusted in weight to produce a scaled downcomer mass and center of gravity.

3.4 VENT HEADER INSTRUMENTATION

The vent header instrumentation, shown in Figure 3-6, consists of eight impact pressure transducers, a transducer to measure pressure inside the cylinder, a load cell and accelerometers to measure vertical force and acceleration, and four strain gauges (used only on the flexible header). The strain gauges were mounted symmetrically in pairs on the inside and outside shell surfaces. The output of each pair was subtracted electronically and the difference between internal and external hoop strain was measured. The gauges measured circumferential bending stress, but not membrane stress.

The eight miniature pressure transducers were distributed over one quadrant of the vent cylinder to characterize the shape of the impact pressure in space and time. Kulite model CQ-140-100A sensors, chosen for their light weight and small size, were mounted with negligible effects on the flexibility, structural integrity and dynamic response of the vent header.

The output from the eight impact pressure transducers and the strain gauges was recorded on high frequency FM tape. Because the impact pressure pulse was narrow, a 4-kHz data sampling rate was used for the vent header instrumentation. A 10-Hz timing signal was also recorded so that the FM data could be related to the digitally sampled data, such as that from the vent header load cell. After the test the FM data was digitized at a 4-kHz sampling rate and displayed both graphically and digitally.

A complete list of the instrumentation, including both basic test facility and additional vent header instrumentation, is given in Table 3-1. This table shows the transducer type and accuracy together with the data sampling rate used for each. The location of each sensor is shown schematically in Figures 3-2 and 3-6.

In addition to the measurements described above, the dimensions of the flexible vent header were recorded manually before and after each test. The measurements, shown in Figure 3-7, were designed to detect any permanent deformation.

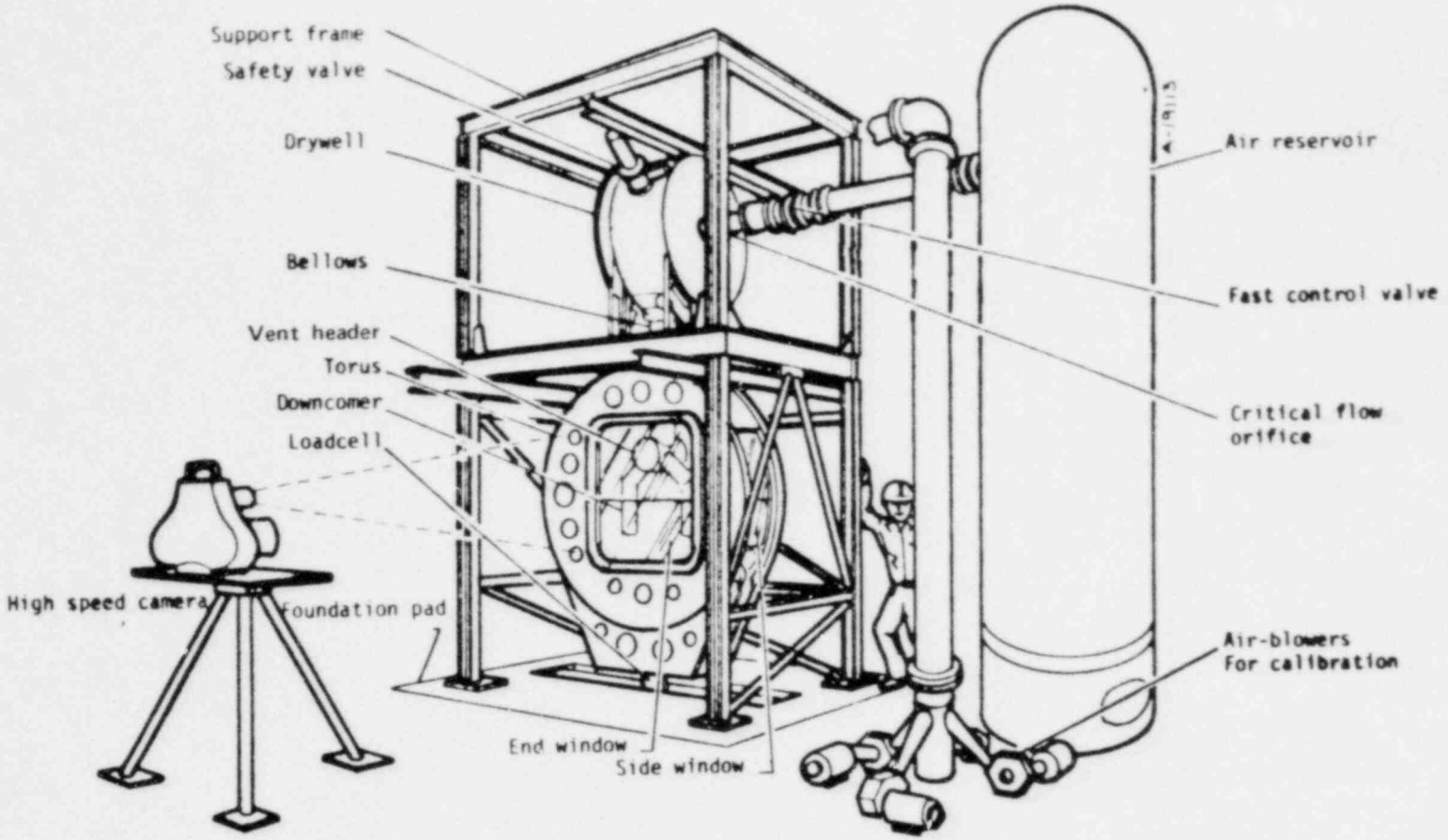

Figure 3-1
Mark I BWR Containment Pool Swell Quarter-scale Test Facility

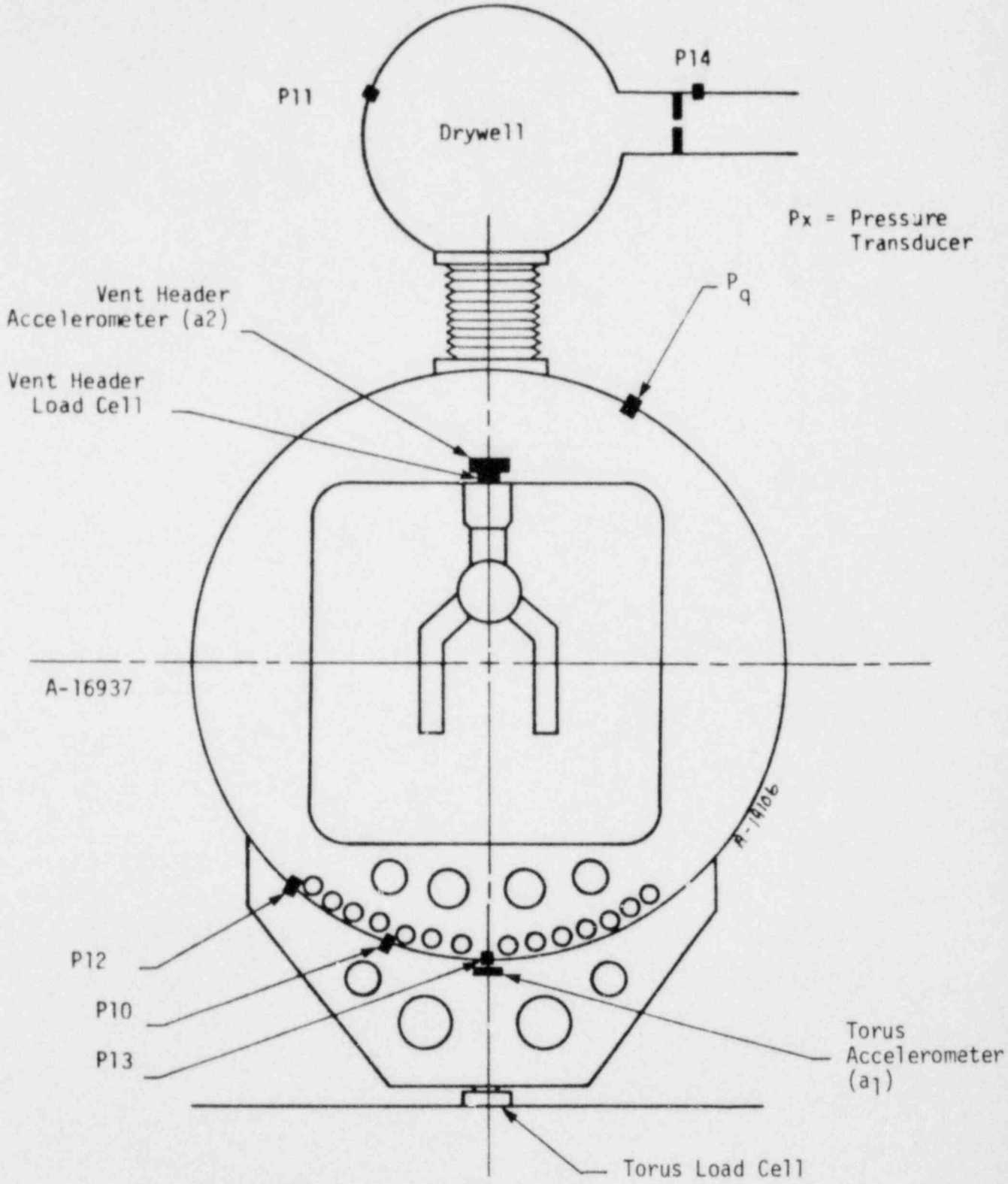

Figure 3-2
Basic Quarter-scale Test Facility Instrumentation

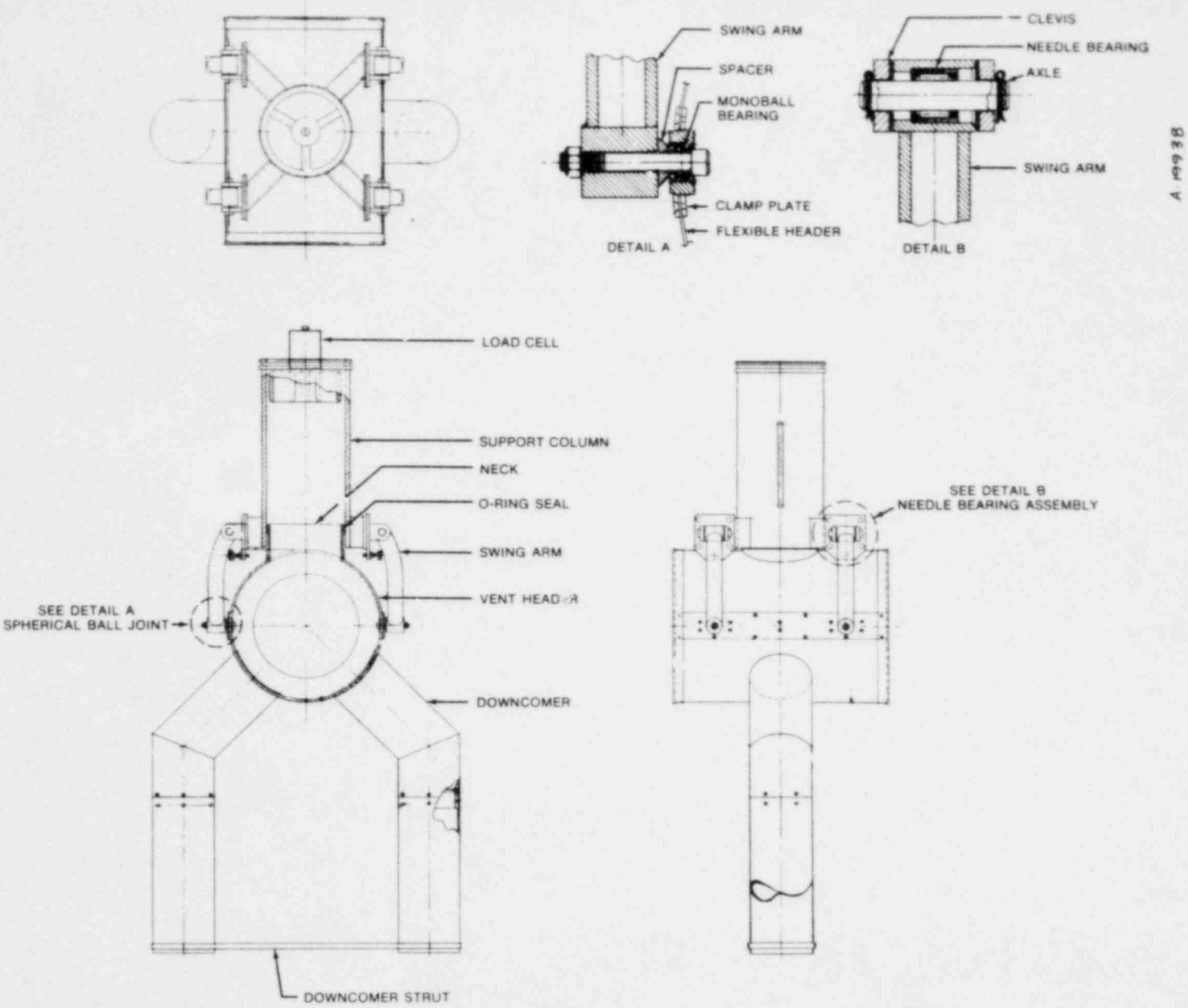

Figure 3-3
Flexible Vent Header and Support System

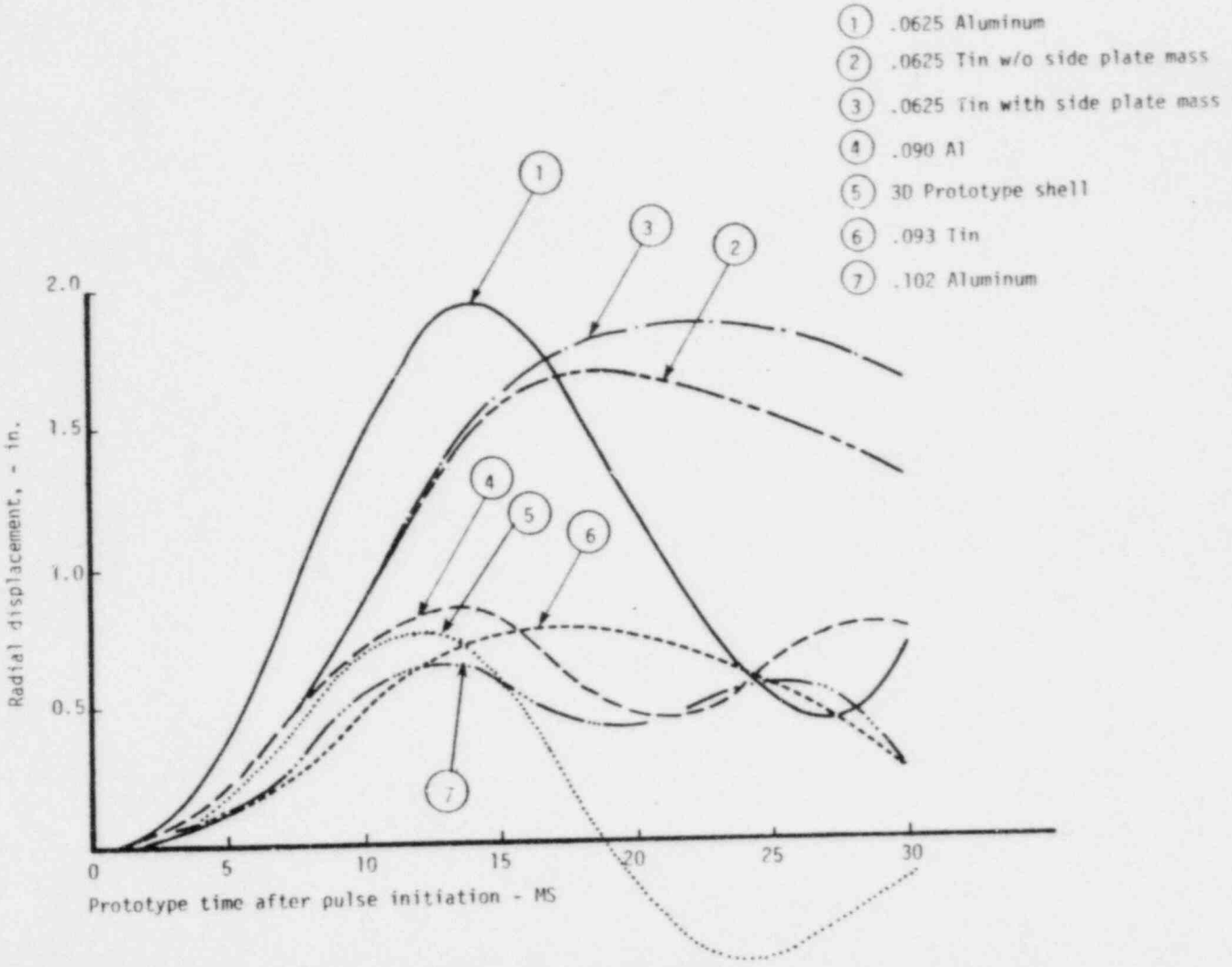

Figure 3-4
Radial Displacement at Bottom Dead Center, 50° Parabolic
Pressure Pulse of 15 MS Duration

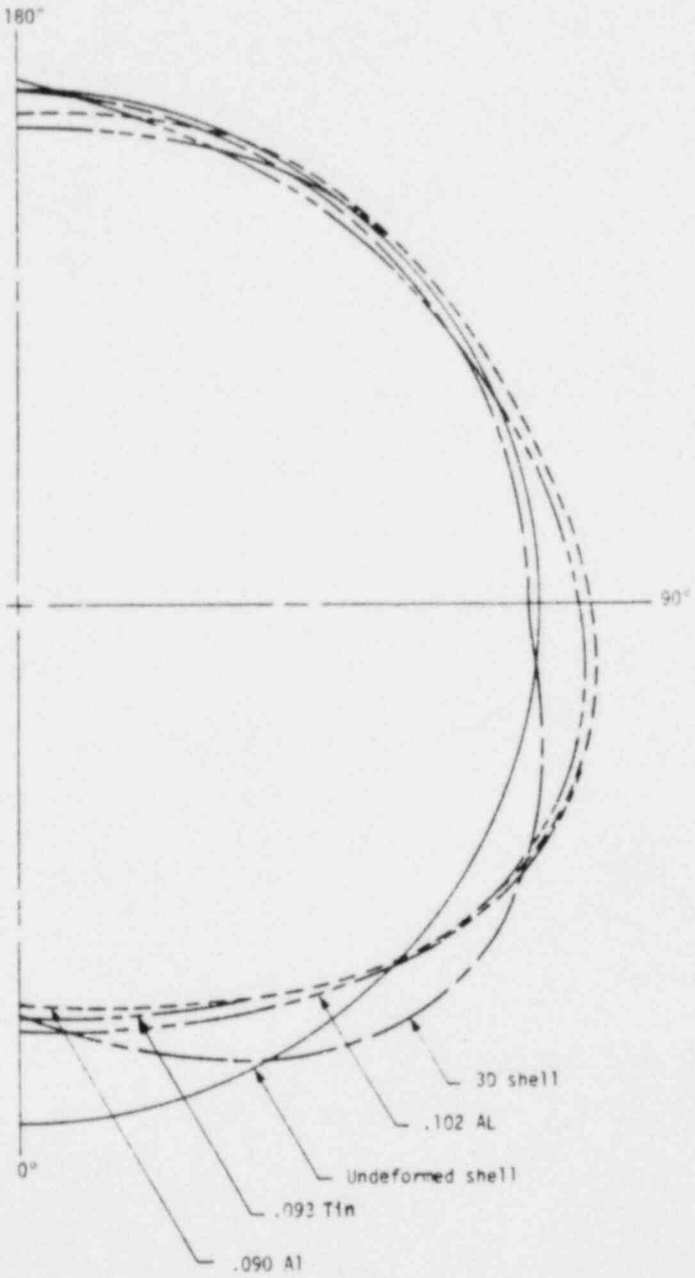

Figure 3-5
Deformed Shape at Maximum Radial Deflection

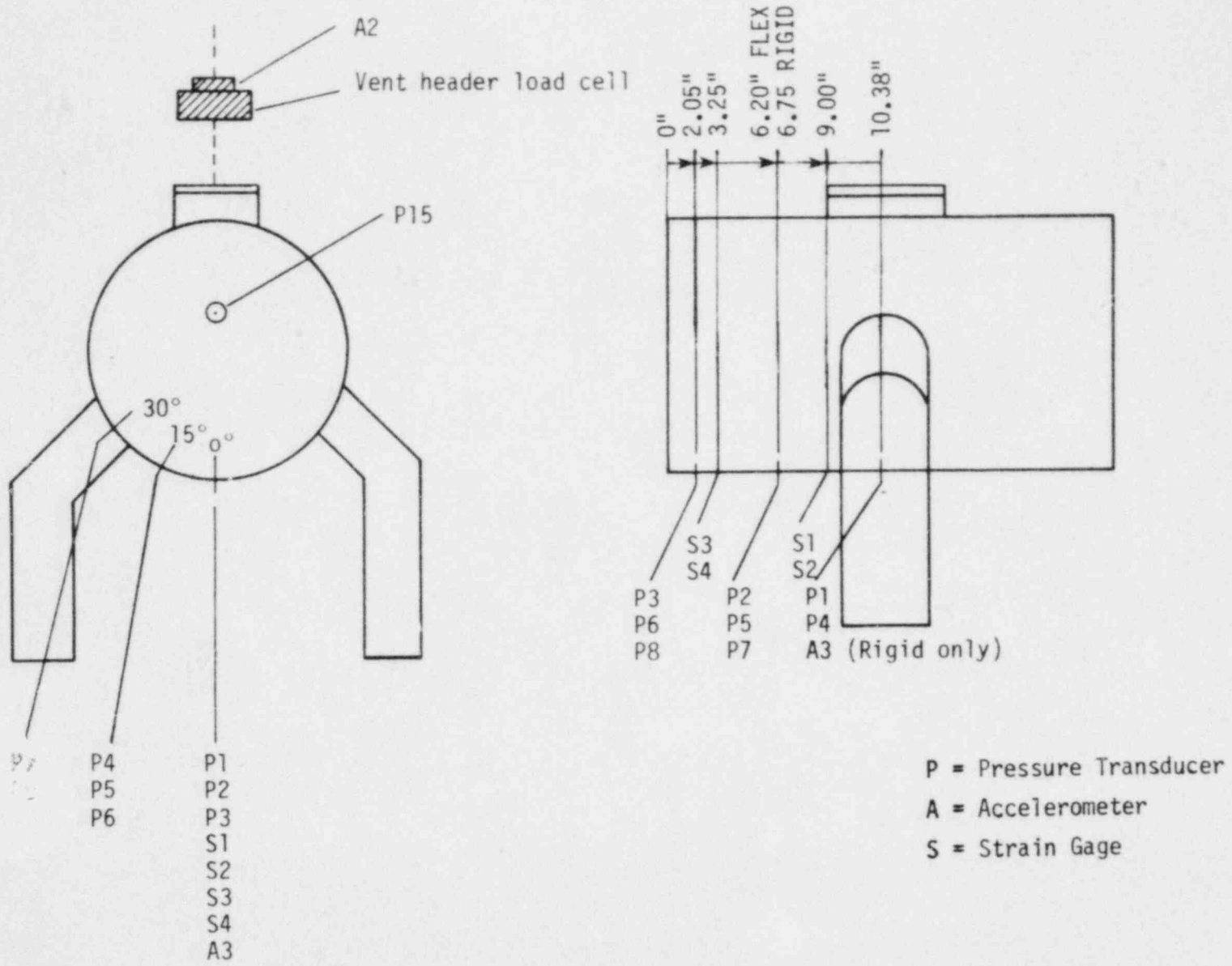

Figure 3-6
Vent Header Instrumentation

Table 3-1
INSTRUMENTATION LIST

A/D CH	Measurement	Location	Sample Rate	Transducer Type	Range	Accuracy
0	Pressure	ww-30°(P9)	500	Senso-metrics SP-65D	0-50 psia	± 0.03 psia
1	Pressure	R/H -(P1)	FM	Kulite CQ-140-100A	0-100 psia	± 0.05 psia
2	Pressure	R/H -(P2)	FM	Kulite CQ-140-100A	0-100 psia	± 0.05 psia
3	Pressure	R/H - (P3)	FM	Kulite CQ-140-100A	0-100 psia	± 0.05 psia
4	Strain	S1 - 52*	FM	Micro-measurements CEA-13	0-10,000 μstrain	± 5 μ-strain
5	Pressure	R/H - (P4)	FM	Kulite CQ-140-100A	0-100 psia	± 0.05 psia
6	Pressure	R/H - (P5)	FM	Kulite CQ-140-100A	0-100 psia	± 0.05 psia
7	Pressure	ww-210°(P10)	500	Senso-metrics SP-65D	0-50 psia	± 0.03 psia
8	Pressure	R/H - (P6)	FM	Kulite CQ-140-100A	0-100 psia	± 0.05 psia
9	Pressure	Drywell (P11)	500	Senso-metrics SP-65D	0-50 psia	± 0.03 psia
10	Pressure	ww-240°(P12)	500	Senso-metrics SP-65D	0-50 psia	± 0.03 psia
11	Pressure	R/H - (P7)	FM	Kulite CQ-140-100A	0-100 psia	± 0.05 psia
12	Pressure	R/H - (P8)	FM	Kulite CQ-140-100A	0-100 psia	± 0.05 psia
13	Pressure	ww-180°(P13)	500	Senso-metrics SP-65D	0-50 psia	± 0.03 psia
14	Pressure	Orifice (P14)	500	Senso-metrics SP-65D	0-100 psia	± 0.06 psia
15	Pressure	R/H (P15)	2 KC	Kulite CQ-140-100A	0-100 psia	± 0.05 psia
16	Load	Torus	2 KC	Interface 1221	50,000 lbs	± 50 lbs
17	Load	Ring Header	2 KC	Interface 1210	10,000 lbs	± 10 lbs
18	Acceleration	Torus (a1)	1 KC	Setra 117	0 to ± 5g	± 0.025g
19	Acceleration	Vent Header (a2)	2 KC	Setra 117	0 to ± 5g	± 0.025g
20	Strain	S3 - S4*	FM	Micro-measurements CEA-13	0-10,000 μ-strain	± 5 μ-strain
21						
22						
23	Acceleration	Vent Header (a3)**	2 KC	Setra 117	0 to ± 25g	± 0.25g

*Flexible only
**Rigid only

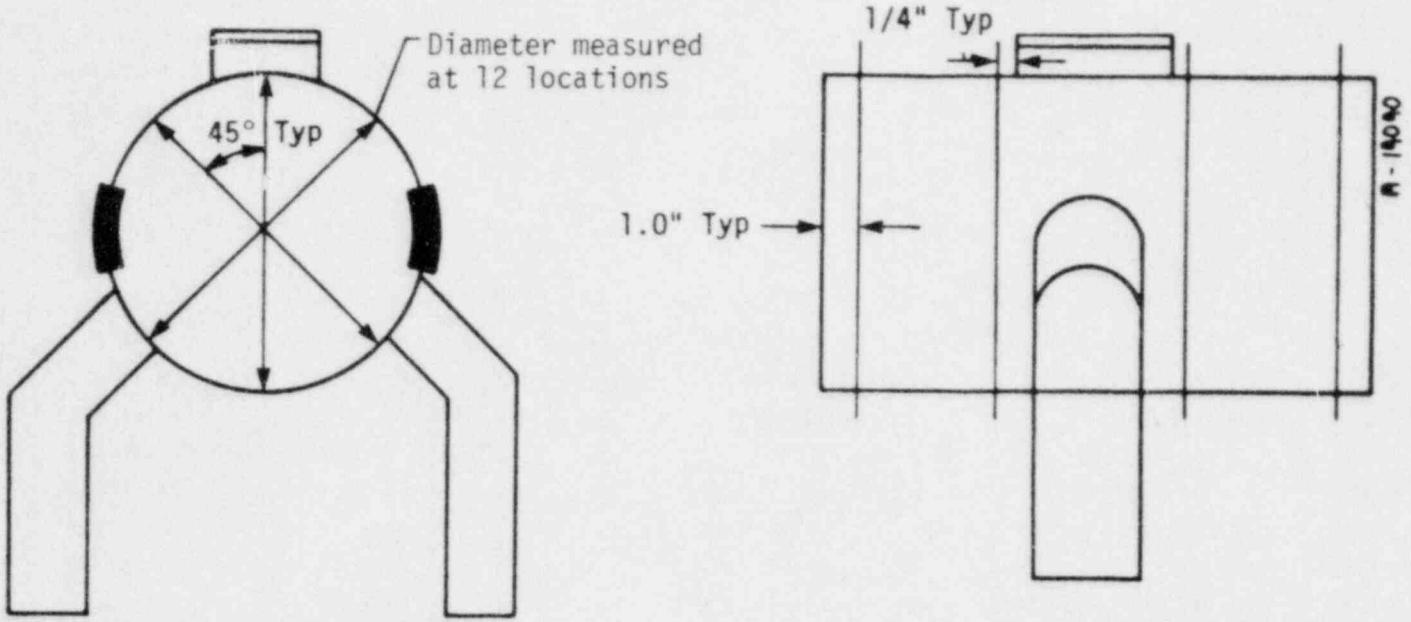

Figure 3-7
Post-test Dimensional Check

4. TEST CONDITIONS AND PROCEDURES

4.1 fL/D MEASUREMENT

The test program started with three quasi-steady fL/D runs to size the vent and downcomer orifices. A quasi-steady fL/D run is performed by removing the main door of the Quarter-scale Test Facility and allowing the facility air supply tank to discharge through the vent system for approximately 15 seconds. The digital data acquisition system measures the following:

a) drywell orifice up stream pressure, P14

b) drywell orifice up stream temperature

c) drywell pressure, P11

d) vent header pressure, P15

e) barometric pressure (recorded manually)

After a 1 second transient, the drywell reaches about 22 psia and the whole facility blows down in a quasi-steady fashion, executing a slow sweep in drywell to ambient pressure ratio (.67 → 1.0).

Each run was manually reduced by calculating the mass rate through the drywell orifice using conventional choked and (later in time) unchoked steady flow equations. Using the calculated mass rate and measured pressure drops, fL/D was calculated.

After determining the deviations of measured and required fL/D, the orifice plates were trimmed to the new estimated diameters. A second quasi-steady run was performed, and the orifice plates resized. A third test-run confirmed the second sizing.

4.2 TEST CONDITIONS AND TEST MATRIX

The test series consisted of 16 test runs: the first eight tests were performed with the rigid aluminum vent header, the remaining tests with the flexible aluminum unit. Both headers were tested at high-load and low-load conditions. One additional test was conducted on the flexible header at an intermediate load condition.

All tests were conducted with nominal quarter-scale facility geometry, i.e., 22-inch pool width and 12-inch downcomer submergence (4 feet in full scale). The loading condition was varied by changing the drywell charging rate and the initial drywell/wetwell differential pressure. The test matrix is shown in Table 4-1 and the nominal facility configuration parameters are listed in Table 4-2.

Table 4-1
TEST MATRIX

Test	Ring Header	Load Condition	Drywell Charging Orifice*	Initial Drywell/ Wetwell ΔP (inches H_2O)
1	Rigid	High	Large	0
2	Rigid	High	Large	0
3	Rigid	High	Large	0
4	Rigid	High	Large	0
5	Rigid	Low	Intermediate	12
6	Rigid	Low	"	12
7	Rigid	Low	"	12
8	Rigid	Low	"	12
9	Flexible	Low	"	12
10	Flexible	Low	"	12
11	Flexible	Low	"	12
12	Flexible	Low	"	12
13	Flexible	Intermediate	"	0
14	Flexible	High	Large	0
15	Flexible	High	"	0
16	Flexible	High	"	0

*Large: 2.668 inch dia.

Intermediate: 2.242 inch dia.

Table 4-2
NOMINAL FACILITY PARAMETERS

Drywell Volume	55 cu. ft. nom.
Wetwell Width	22 inches
Water Level	3 inches below wetwell $\mathbb{Q}$
Downcomer submergence	12 inches
Torus initial pressure	3.68 ± 0.02 psia
Reservoir initial pressure	40 ± 0.2 psig
Water surface tension	35 ± 5 dynes/cm
Torus vertical frequency	~ 53 cps
Distributed vent resistance	Orifice diameters $\begin{cases} D_{vent} = 6.193 \text{ in.} \\ D_{downcomer} = 3.778 \text{ in.} \end{cases}$

A window-stiffening strut was included and surfactant was added to the pool to reduce download oscillations caused by window vibration and the presence of air bubbles on the wetwell surfaces. A vertical natural frequency of 53 Hz for the torus was maintained on all tests.

5. DATA REDUCTION

5.1 STANDARD DATA REDUCTION

Data for this series of tests fell into two categories: data specifically related to vent header loads (impact pressures and strain measurements) and data which characterize the test condition such as vertical torus loads (to ensure that nominal test conditions were achieved).

In the standard data package for each test, data from each instrumentation channel including all pressure, temperature, acceleration and load data, are displayed both graphically as a function of time and digitally in a listing. In addition, several plots and listings of calculated data are produced. These include:

1. Torus pressure integral - an area integral of pressure around the circumference of the wetwell

2. Acceleration corrected pressure integral - the torus pressure integral minus the mass of the water times its vertical acceleration. This most closely represents the true vertical driving force for a rigid facility.

3. Torus impulse - a time integral of (1)

4. Enthalpy flux into the wetwell

5. Torus Force - the torus load cell output minus mass of torus time acceleration. This is comparable to (1)

6. Vent Header Force - vent header load cell minus mass of vent header times acceleration

7. Vent Header Impulse - time integral of (6).

An area integration of the individual vent header impact pressures was performed to determine the vertical vent header load. This technique is discussed in the following section.

5.2 IMPACT PRESSURE INTEGRAL METHOD

A special technique was developed during this program to integrate the measured vent-header impact pressures to obtain force. Eight transducers were distributed in one quadrant of the vent header in the region from bottom dead center (BDC) to 30° from BDC, see Figure 3-6. Eight locations were not sufficient to produce a smooth integral and a scheme for interpolating to construct pressure histories at intermediate locations was developed.

Figure 5-1 is a schematic example of the interpolation technique. Assume positions A, B, C, and D are to be interpolated from positions

1, 2, and 3. The measurements at 1, 2, and 3 are approximated by 3 straight line segments as shown in Figures 5-2, 5-3 and 5-4, from Test 1. Each function then has four points shown in Figure 5-1 such as 1-1, 1-2, 1-3, 1-4, 2-1, 2-2, 2-3, 2-4 etc. Since the wave speed was observed to be nonlinear, the times of occurrence of similiar points of the wave (e.g., 1-2, 2-2, 3-2) were fit to a quadratic and the times of intermediate points determined from these curves, Figure 5-5. Intermediate pressure values such as A-2 and B-2, were linearly interpolated between values 1-2 and 2-2, etc. Both linear and quadratic fits were tried for interpolating the pressure values with negligible effect on the integral; the linear method was retained.

This procedure was carried out for intermediate zones between points 4, 5 and 6 and between 7 and 8. For points to the right of 3, 6 and 8, analytic extensions of the time and pressure functions were used. The grid size was refined until significant changes in the integral ceased. The final grid configuration used is shown in Figures 5-6 and 5-7. Two configurations were required since transducer locations were not identical in the rigid and flexible models. The angular extent of the zones centered at 30° was assumed to be 22.5° to 37.5°. This assumption is arbitrary and was justified by 1) the fact that the value of the pulse was decaying with θ and extrapolated to zero near 40-45° for the rigid case and 2) the reasonably good agreement of the pressure integral impulse and the load cell impulse.

As shown in Figure 6-16 in Section 6, there is a double spike for P4. The first spike is judged to be caused by a local water jet which sweeps up the angled downcomer and impacts the local area around the transducer. Because its area of influence in the movies was observed to be small, it was eliminated in the four point characterization of P4. Likewise, some of the fine structure, such as the second spike in P1, was eliminated, perserving the impulse.

Load contribution due to impact with the angled downcomers was ignored, since the water strikes the downcomer at 45° and little impact pressure is expected at this angle (note that the impact pressure was extrapolated to zero at θ = 40-45° on the cylinder).

5.3 POOL IMPACT VELOCITY DETERMINATION

The velocity of the rising wetwell pool at vent header impact was determined from the high-speed photographs. Each frame of the film is marked with a digital time referenced to test beginning. By projecting the film and marking the pool location at various times prior to impact, pool heignt can be graphed as a function of time. Differentiating this curve will yield the pool velocity at any selected time. The velocity values reported in Section 6 are for times just prior to impact.

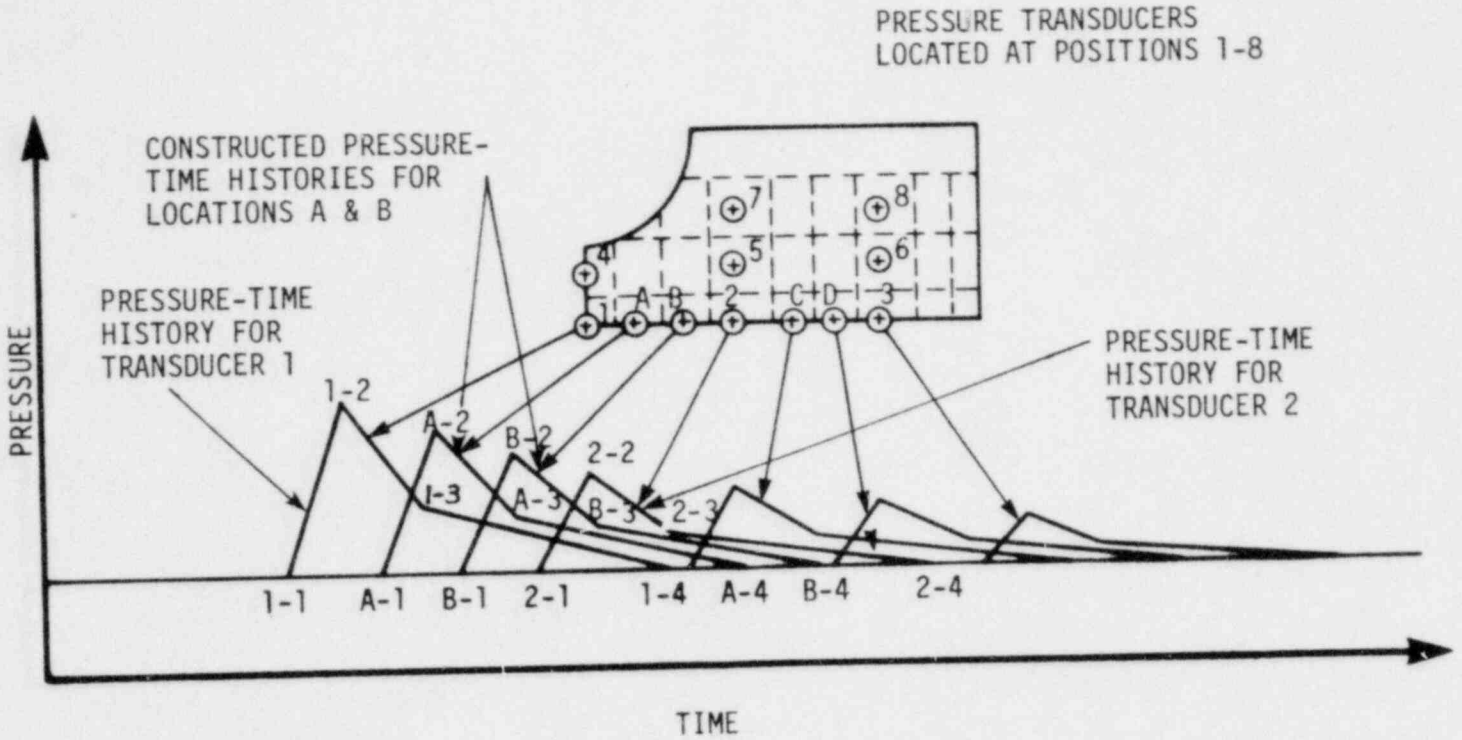

Figure 5-1
Vent Header Pressure Interpolation Technique

GE Company Proprietary

Figure 5-2
Impact Pressure Profile
(GE Company Proprietary)

GE Company Proprietary

Figure 5-3
Impact Pressure Profile
(GE Company Proprietary)

GE Company Proprietary

Figure 5-4
Impact Pressure Profile
(GE Company Proprietary)

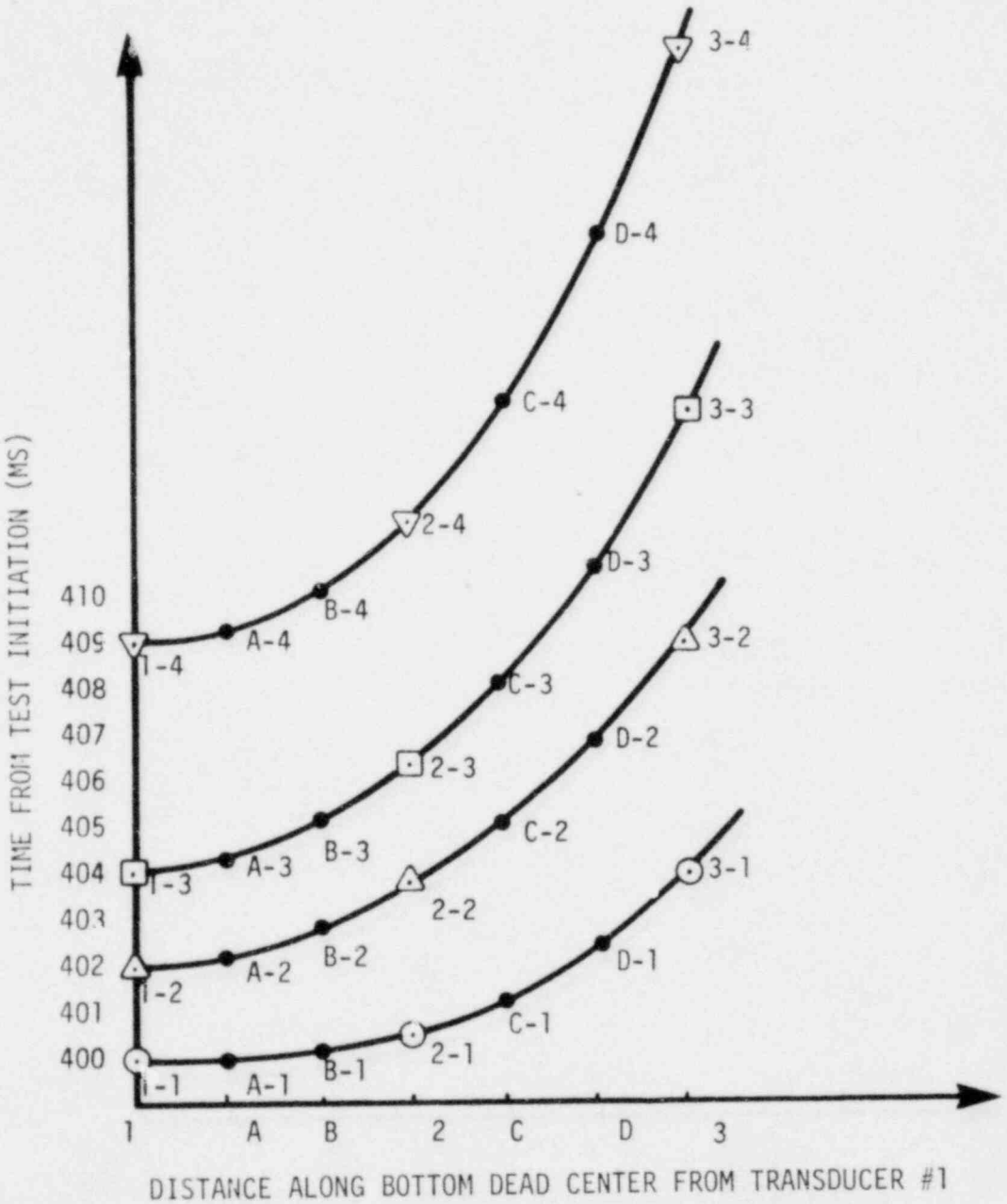

Figure 5-5
Time of Arrival of Points 1, 2, 3, and 4 of the Generalized Wave as a Function of Location (See Figure 5-2)

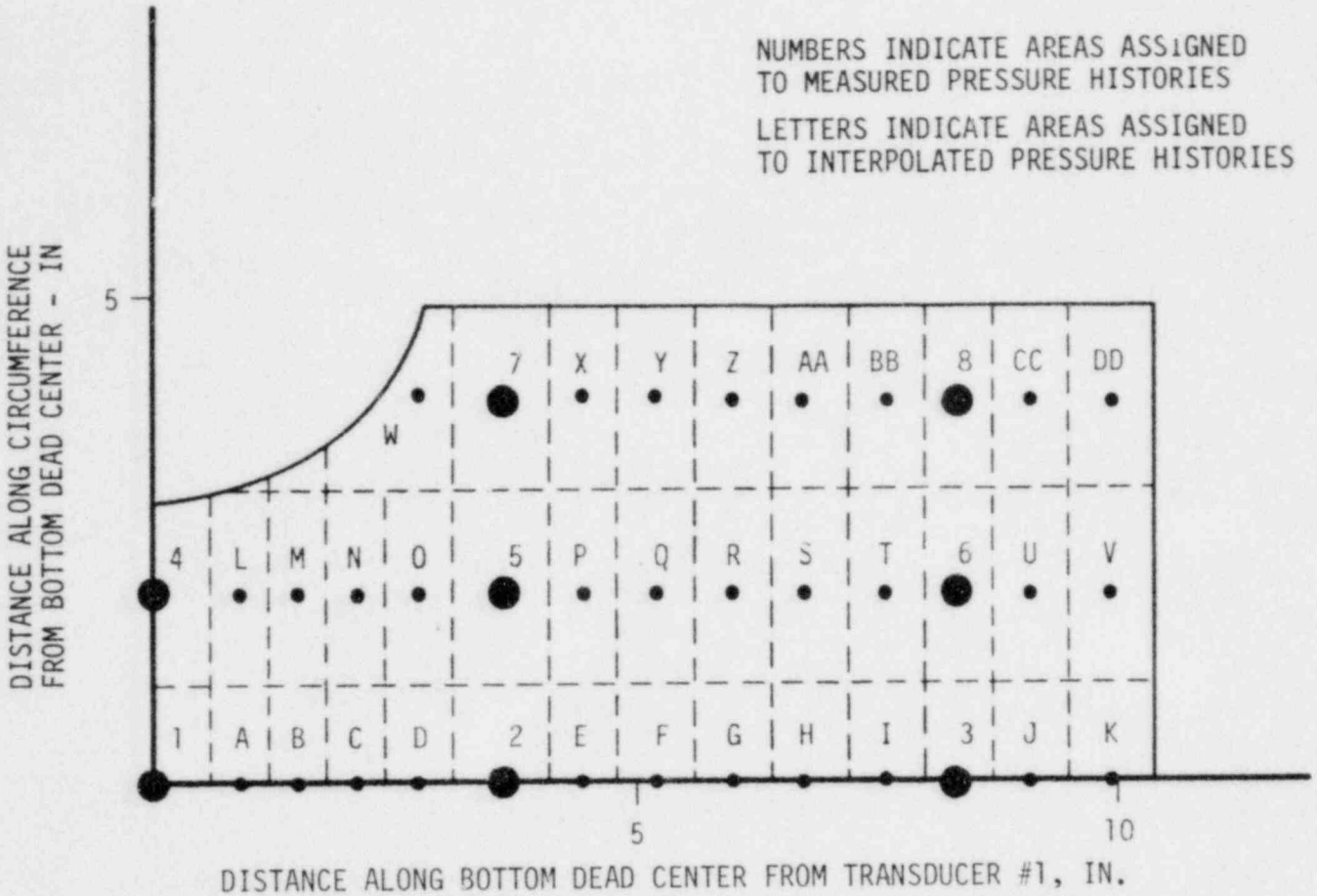

Figure 5-6
Rigid Vent Header Mesh Configuration

6. TEST RESULTS AND CONCLUSIONS

6.1 TYPICAL PRESSURE MEASUREMENTS

Typical pressure data from high- and low-load rigid tests and high- and low-load flexible tests are shown as Figure 6-1 thru 6-4. The flexibility generally lowers and broadens the pressure pulse along the bottom dead center stations (P1, P2, and P3), and at the 15° stations (P4, P5, and P6). This effect is more pronounced at the high-load condition. The effect at the 30° station (P7 and P8) is ambiguous and in some cases shows a sharper spike for the flexible model. This could be due to: 1) the influence of the deformed ring header shape on the impact at 30°, 2) alteration in the spray pattern from the impact at BDC due to flexibility, or 3) some variation in the pool surface shape due to small differences between the two models.

6.2 PRESSURE INTEGRALS

The results of integration of the eight impact pressure transducer readings to vent header force is shown in Figures 6-5 thru 6-18. Tests 8 and 13 were not reduced since the pressure history at an important location was lost when the transducer malfunctioned. P8, a less critical location, was lost for runs 4-8. The P8 data from run 1 was used with the appropriate time adjustment for the integration of run 4. The P8 value from run 9 was used for runs 5-8.

Table 6-1 summarizes the average peak loads and impulse obtained from the pressure integrals.

Table 6-1
IMPACT LOAD MEASUREMENT SUMMARY
(GE Company Proprietary)

(GE Company Proprietary)

6.3 LOAD CELL RESULTS

Figure 6-19 shows the flexible vent header load measurement system. The new system made use of the existing load cell and the load path above the cell consisting of a column and spider to the drywell flange. Flexibility in this path above the load cell limited the maximum first vertical natural frequency to approximately 90 Hz in the existing system. Since the new vent header models were lighter the first vertical mode was improved to about 110-120 Hz. This proved to be appropriate for measuring the reaction loads for the flexible model, since the ovalling mode of the flexible model limits the frequency of the reaction load to about 60 Hz. Since the rise time of the rigid loading function is about 1 ms no amount of practical improvement in the load system natural frequency would have helped the rigid measurement.

A multimass analytical model of the vent header load measurement system was constructed to see if the measured load cell response could be predicted using the measured pressure integral loads. A two mass model was used for the rigid system. The first spring/mass was the vent header/swing arms. The second spring/mass was the support tube/load cell and load path to the drywell flange. In the flexible model a 3rd spring/mass was added representing the vent header ovalling inertia and stiffness.

Results of this analysis are compared to load cell response for four representative runs in Figures 6-20 thru 6-23. Dynamic amplification occurred in all cases. For the rigid header, the amplification is caused by the spring/mass of the measurement system, i.e., the swing arms and load cell path, and therefore is not relevant. The amplification for the flexible header is principally due to the ovalling spring/mass. This was verified by inputting the same F(t) to a single spring/mass system which modeled the ovalling mode only -- the equivalent of making the measurement system springs infinitely stiff. The result of this analysis is plotted on Figures 6-22 and 6-23, and the load cell response is nearly the same for the 1 mass and 3 mass models. Hence, the influence of the measurement system is minor for the flexible case and the measured reaction loads are essentially correct.

The load cell results for the eight flexible runs are shown as Figures 6-24 thru 6-31. Table 6-2 lists the load cell peak loads for 8 flexible runs and impulses for all 16 runs.

6.4 POOL SWELL VELOCITIES

The pool swell velocities just prior to impact were obtained from high speed movies. Results are summarized in Table 6-3, comparing data from this test program to earlier data from Part I of the Quarter-scale Test Program.

6.5 STRAIN GAGE RESULTS

The strain channels were reset prior to the next test. The diminishing strain offset is judged to be due to strain hardening. Pre- and post-test diameter measurements did not show any measurable ovalling deformation. Peak strains, strain offset and dimensional data are presented in Tables 6-4 and 6-5.

6.6 TORUS RESULTS

In this program torus loads were also measured in the 16 tests. This was first of the series in which any torus data was obtained with the fL/D split between the vent and downcomers. Also, download oscillations had been present in previous Quarter-scale torus data and its elimination was the subject of a separate study. This series was the first to use both a window brace and pool surfactant and the amount of residual oscillation was predicted to be low. A window brace consists of a strut set between the two plexiglas windows, limiting the window deflection.

Figure 6-33 shows a comparison of a typical torus force plot with two earlier runs. One of the comparison runs, II-3-04, is with no brace and no surfactant. The second comparison, run II-3-09, is with 10 struts and surfactant. The download oscillations for this program appear to be almost as small as the 10 strut case, run II-3-09. The general agreement shown in Figure 6-33 between the torus force from this series and series II-3 (which did not have split fL/D) leads to the conclusion that the split fL/D has no measurable effect.

The average download and upload for this program is shown in Table 6-6.

GE Company Proprietary

Figure 6-1
Pressure Measurements, High-load, Rigid
(GE Company Proprietary)

GE Company Proprietary

Figure 6-2
Pressure Measurements; High-load, Flexible
(GE Company Proprietary)

GE Company Proprietary

Figure 6-3
Pressure Measurements; Rigid, Low-load
(GE Company Proprietary)

GE Company Proprietary

Figure 6-4
Pressure Measurements; Flexible, Low-load
(GE Company Proprietary)

GE Company Proprietary

Figure 6-5
Impact Load Measurements; Rigid, High-load
(GE Company Proprietary)

GE Company Proprietary

Figure 6-6
Impact Load Measurements; Rigid, High-load
(GE Company Proprietary)

GE Company Proprietary

Figure 6-7
Impact Load Measurements; Rigid, High-load
(GE Company Proprietary)

GE Company Proprietary

Figure 6-8
Impact Load Measurements; Rigid, High-load
(GE Company Proprietary)

GE Company Proprietary

Figure 6-9
Impact Load Measurements; Rigid, Low-load
(GE Company Proprietary)

GE Company Proprietary

Figure 6-10
Impact Load Measurements; Rigid, Low-load
(GE Company Proprietary)

GE Company Proprietary

Figure 6-11
Impact Load Measurements; Rigid, Low-load
(GE Company Proprietary)

GE Company Proprietary

Figure 6-12
Impact Load Measurements; Flexible, Low-load
(GE Company Proprietary)

GE Company Proprietary

Figure 6-13
Impact Load Measurements; Flexible, Low-load
(GE Company Proprietary)

GE Company Proprietary

Figure 6-14
Impact Load Measurements; Flexible, Low-load
(GE Company Proprietary)

GE Company Proprietary

Figure 6-15
Impact Load Measurements; Flexible, Low-load
(GE Company Proprietary)

GE Company Proprietary

Figure 6-16
Impact Load Measurements; Flexible, High-load
(GE Company Proprietary)

GE Company Proprietary

Figure 6-17
Impact Load Measurements; Flexible, High-load
(GE Company Proprietary)

GE Company Proprietary

Figure 6-18
Impact Load Measurements; Flexible, High-load
(GE Company Proprietary)

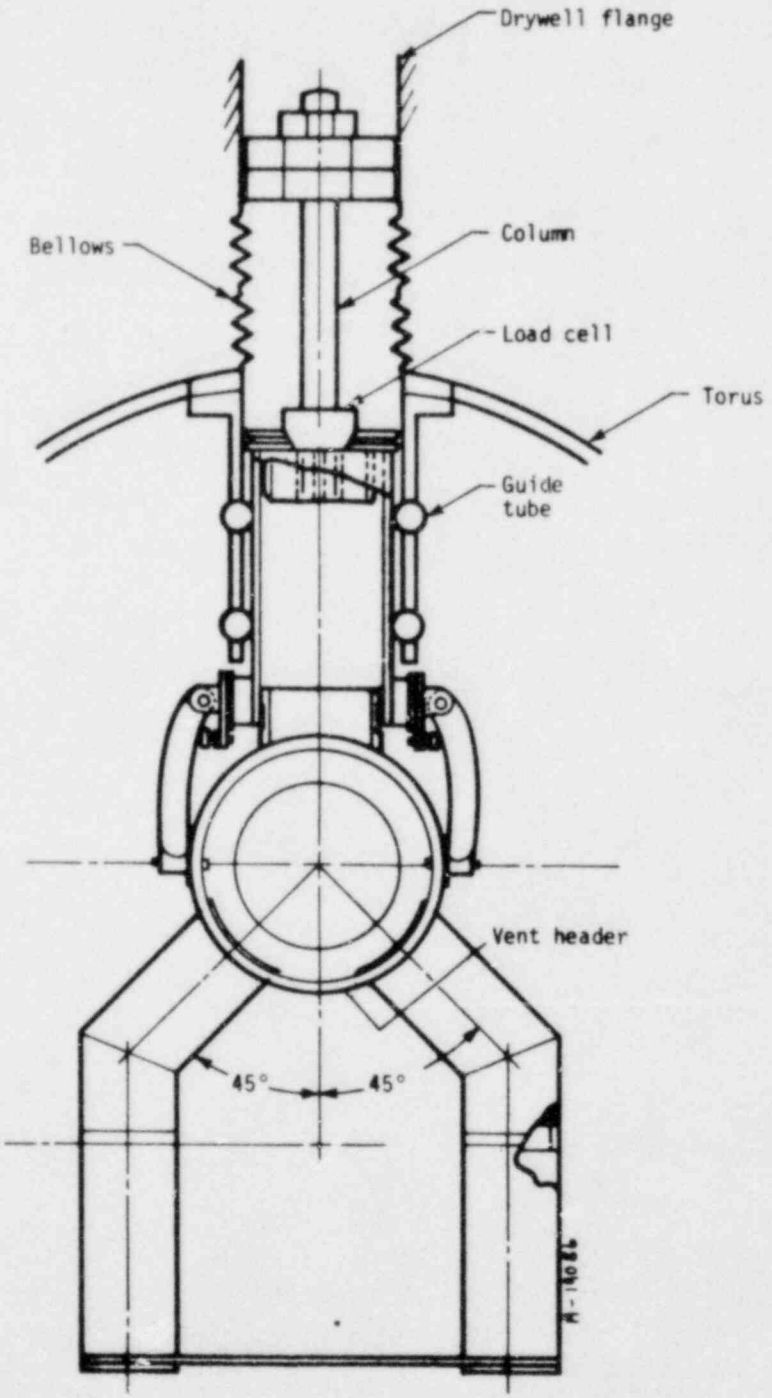

Figure 6-19
Vent Header Support Arrangement

GE Company Proprietary

Figure 6-20
Comparison of Measured and Calculated Load Cell Response
Using the Pressure Integral Force as Input, Test 4
(GE Company Proprietary)

GE Company Proprietary

Figure 6-21
Comparison of Measured and Calculated Load Cell Response
Using the Pressure Integral Force as Input, Test 5

GE Company Proprietary

Figure 6-22
Comparison of Measured and Calculated Load Cell Response
Using the Pressure Integral Force as Input, Test 9
(GE Company Proprietary)

GE Company Proprietary

Figure 6-23
Comparison of Measured and Calculated Load Cell Response
Using the Pressure Integral Force as Input, Test 14
(GE Company Proprietary)

GE Company Proprietary

Figure 6-24
Vent Header Load Cell Profile
(GE Company Proprietary)

GE Company Proprietary

Figure 6-25
Vent Header Load Cell Profile
(GE Company Proprietary)

GE Company Proprietary

Figure 6-26
Vent Header Load Cell Profile
(GE Company Proprietary)

GE Company Proprietary

Figure 6-27
Vent Header Load Cell Profile
(GE Company Proprietary)

GE Company Proprietary

Figure 6-28
Vent Header Load Cell Profile
(GE Company Proprietary)

GE Company Proprietary

Figure 6-29
Vent Header Load Cell Profile
(GE Company Proprietary)

GE Company Proprietary

Figure 6-30
Vent Header Load Cell Profile
(GE Company Proprietary)

GE Company Proprietary

Figure 6-31
Vent Header Load Cell Profile
(GE Company Proprietary)

Table 6-2
VENT HEADER LOAD CELL RESULTS
(GE Company Proprietary)

GE Company Proprietary

Table 6-3
POOL SWELL VELOCITIES (ft/s)
(GE Company Proprietary)

GE Company Proprietary

GE Company Proprietary

Figure 6-32
Vent Header Strain Histories
(GE Company Proprietary)

Table 6-4
PEAK STRAINS IN FLEX CYL TESTS
(GE Company Proprietary)

GE Company Proprietary

Table 6-5
POST TEST DIMENSIONS AND STRAIN OFFSETS
(GE Company Proprietary)

GE Company Proprietary

*Strain readings reset to zero prior to subsequent test.

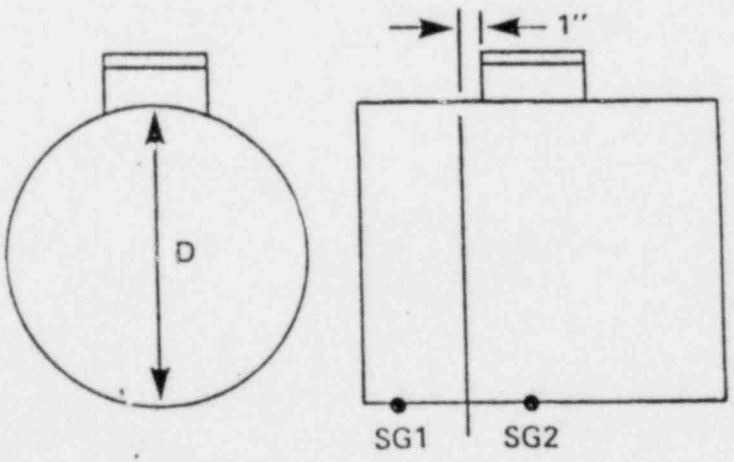

GE Company Proprietary

Figure 6-33
Comparison of Torus Loads of a Typical Test in the "Rigid and Flexible Vent Header Program" to Two Tests of Series II-3 with Comparable Test Conditions
(GE Company Proprietary)

Table 6-6
TORUS LOADS
(GE Company Proprietary)

GE Company Proprietary

7. REFERENCES

1. Von Karman, T., "The Impact of Seaplane Floats During Landing," NACA TN-321, 1929.

2. Madden, R., Progress Report #18, NASA Contract NASB-23618, 11 June 1974.

3. Ochi, M. D., Schwartz, F. M., Two-Dimensional Experiments on the Effect of Hull Form on Hydrodynamic Impact, Dept. of the Navy Report 1994, May 1966.

4. Mark I Containment Evaluation, Short Term Program Final Report Volume II LOCA-related Hydrodynamic Loads, NEDC-20989-2P, September 1975.

5. Torbeck, J. E., et al., Mark I 1/12-Scale Pressure Suppression Pool Swell Tests, March 1976, (NEDE - 13456-P).

6. D. L. Galyardt, C. G. Hayes and S. L. Kushman, Mark I Containment Program 1/4 Scale Pressure Suppression Pool Swell Test Program: Scaling Evaluation, NEDE-21627-P, General Electric, January 1978.

7. James, A. J., and Libkind, M. A., Calculation of Overall Flow Loss Coefficient for the Vent System of a Torus/Lightbulb Containment. General Electric Company Report NEDO-10320, January 1973.